







## Article

# Phytocannabinoids: Chromatographic Screening of Cannabinoids and Loading into Lipid Nanoparticles

Aleksandra Zielińska<sup>1,2,\*</sup>, Raquel da Ana<sup>2</sup>, Joel Fonseca<sup>2</sup>, Milena Szalata<sup>3</sup>, Karolina Wielgus<sup>4</sup>, Faezeh Fathi<sup>5</sup>, M. Beatriz P. P. Oliveira<sup>5</sup>, Rafał Staszewski<sup>6</sup>, Jacek Karczewski<sup>7,8</sup> and Eliana B. Souto<sup>2,9,10,\*</sup>

<sup>1</sup> Institute of Human Genetics, Polish Academy of Sciences, Strzeszyńska 32, 60-479 Poznan, Poland

<sup>2</sup> Department of Pharmaceutical Technology, Faculty of Pharmacy, University of Porto, Rua de Jorge Viterbo Ferreira, 228, 4050-313 Porto, Portugal

<sup>3</sup> Department of Biotechnology, Institute of Natural Fibres and Medicinal Plants, National Research Institute, Wojska Polskiego 71B, 60-630 Poznan, Poland

<sup>4</sup> Department of Pediatric Gastroenterology and Metabolic Diseases, Poznan University of Medical Sciences, Szpitalna 27/33, 60-572 Poznan, Poland

<sup>5</sup> REQUIMTE/LAQV, Department of Chemical Sciences, Faculty of Pharmacy, University of Porto, Rua Jorge Viterbo Ferreira No. 280, 4050-313 Porto, Portugal

<sup>6</sup> Department of Hypertension Angiology and Internal Medicine, Poznan University of Medical Sciences, 61-701 Poznan, Poland

<sup>7</sup> Department of Environmental Medicine, Poznan University of Medical Sciences, 61-701 Poznan, Poland

<sup>8</sup> Department of Gastroenterology, Dietetics and Internal Diseases, H. Swiecicki University Hospital, Poznan University of Medical Sciences, 60-355 Poznan, Poland

<sup>9</sup> REQUIMTE/UCIBIO, Faculty of Pharmacy, University of Porto, Rua de Jorge Viterbo Ferreira, 228, 4050-313 Porto, Portugal

<sup>10</sup> Associate Laboratory i4HB—Institute for Health and Bioeconomy, Faculty of Pharmacy, University of Porto, 4050-313 Porto, Portugal

\* Correspondence: [aleksandra.zielinska@igcz.poznan.pl](mailto:aleksandra.zielinska@igcz.poznan.pl) (A.Z.); [esouto@ff.up.pt](mailto:esouto@ff.up.pt) (E.B.S.)



**Citation:** Zielińska, A.; da Ana, R.; Fonseca, J.; Szalata, M.; Wielgus, K.; Fathi, F.; Oliveira, M.B.P.P.; Staszewski, R.; Karczewski, J.; Souto, E.B. Phytocannabinoids: Chromatographic Screening of Cannabinoids and Loading into Lipid Nanoparticles. *Molecules* **2023**, *28*, 2875. <https://doi.org/10.3390/molecules28062875>

Academic Editor: Periakaruppan Prakash

Received: 16 February 2023

Revised: 13 March 2023

Accepted: 20 March 2023

Published: 22 March 2023



**Copyright:** © 2023 by the authors. Licensee MDPI, Basel, Switzerland. This article is an open access article distributed under the terms and conditions of the Creative Commons Attribution (CC BY) license (<https://creativecommons.org/licenses/by/4.0/>).

**Abstract:** Solid Lipid Nanoparticles (SLN) and Nanostructured Lipid Carriers (NLC) are receiving increasing interest as an approach to encapsulate natural extracts to increase the physicochemical stability of bioactives. Cannabis extract-derived cannabidiol (CBD) has potent therapeutic properties, including anti-inflammatory, antioxidant, and neuroprotective properties. In this work, physicochemical characterization was carried out after producing Compritol-based nanoparticles (cSLN or cNLC) loaded with CBD. Then, the determination of the encapsulation efficiency (EE), loading capacity (LC), particle size (Z-Ave), polydispersity index (PDI), and zeta potential were performed. Additionally, the viscoelastic profiles and differential scanning calorimetry (DSC) patterns were recorded. As a result, CBD-loaded SLN showed a mean particle size of  $217.2 \pm 6.5$  nm, PDI of  $0.273 \pm 0.023$ , and EE of about 74%, while CBD-loaded NLC showed Z-Ave of  $158.3 \pm 6.6$  nm, PDI of  $0.325 \pm 0.016$ , and EE of about 70%. The rheological analysis showed that the loss modulus for both lipid nanoparticle formulations was higher than the storage modulus over the applied frequency range of 10 Hz, demonstrating that they are more elastic than viscous. The crystallinity profiles of both CBD-cSLN (90.41%) and CBD-cNLC (40.18%) were determined. It may justify the obtained encapsulation parameters while corroborating the liquid-like character demonstrated in the rheological analysis. Scanning electron microscopy (SEM) study confirmed the morphology and shape of the developed nanoparticles. The work has proven that the solid nature and morphology of cSLN/cNLC strengthen these particles' potential to modify the CBD delivery profile for several biomedical applications.

**Keywords:** solid lipid nanoparticles; nanostructured lipid carriers; cannabidiol; viscoelastic behavior; Compritol® 888 ATO; Miglyol® 812

## 1. Introduction

Lipid nanoparticles are one of the most popular drug delivery systems due to their versatility in loading chemically different active ingredients with high efficiency [1]. The

primary purpose of using these particles is to increase the bioavailability of the loaded drug [2]. There are two types of lipid nanoparticles, namely Solid Lipid Nanoparticles (SLN) and Nanostructured Lipid Carriers (NLC), which are composed exclusively of solid oils and a mixture of solid and liquid oils, respectively [3,4]. Both generations of lipid nanoparticles are composed of two immiscible phases: lipid and water. The main difference in the structure of both nanostructures is the different distribution of the active substance in the space of the lipid matrix. Therefore, their synthesis requires surfactants. The most important properties of lipid nanoparticles include adhesion properties leading to the formation of a hydrophobic film on the skin, which limits the transepidermal water loss and the modified release of drugs [5]. However, the most significant advantages of these drug carriers are their non-toxicity, which results from a biodegradable lipid matrix that undergoes enzymatic degradation to compounds naturally present in the human body [6,7]. SLN and NLC are also relatively easy to obtain and introduce to the market due to the high availability of lipids. The potential toxicity of lipid nanoparticles may depend only on the particle size, the incorporated active substance, and the type of surfactant. Particles exceeding 40 nm cannot penetrate the living cells of the epidermis or the bloodstream and thus do not cause side effects for the body. Only compounds approved by the European Medicines Agency (EMA) and the American Food and Drug Administration (FDA) are on the GRAS list (Generally Recognized As Safe—considered safe).

Lipid nanoparticles are especially interesting for oral administration due to different aspects. Firstly, it should emphasize the mucoadhesive properties that they present due to their colloidal structure, which facilitates drug release in the intestine [8–14]. Additionally, they could be absorbed by the intestinal cells since the lipids composing the nanoparticles have a promoting absorption effect. Many studies have produced lipid nanoparticles to increase the limited oral bioavailability of natural extracts and protect the bioactive compounds loaded from the harsh gastric environments and hepatic first-pass metabolism [6,15–17]. The delayed drug release obtained by SLN and NLC enables the intact presence of the drug in the intestine [18]. Thus, some of the features that make lipid nanoparticles up-and-coming systems for oral administration are providing controlled drug release, protecting drugs from degradation, and improving oral bioavailability of the drug by reducing hepatic first-pass metabolism [19–21].

Moreover, the added value of SLN and NLC encapsulating natural extracts remains in their lipid composition [22,23]. The absorption-promoting effect of lipids has been studied widely, describing the degradation of the lipids by the digestive enzymes resulting in mono and diglycerides that form micelles. In these micelles, the bioactive compounds will be included and interact with the bile salts, resulting in mixed micelles that facilitate the bioactive compound absorption. Indeed, intestinal lymphatic vessels are specialized to assimilate dietary fats as long-chain fatty acids or triglycerides. This feature makes lipid nanoparticles an exciting system for drug targeting [24]. It is shown that triglyceride-based nanoparticles and long-chain rich acids-based nanoparticles may enter the intestinal lymphatic system of the gut [7,22,25]. In this manner, NLC and SLN formulations, including lipids with long-chain fatty acids (containing 12 or more carbon atoms) as Compritol® 888 ATO, which consists of mono-, di- and tri-esters of behenic acid (C22), are described as sound systems to enhance natural extracts' bioavailability [26]. Encapsulation efficiency, smaller particle size, narrow size distribution, and rheological behavior are crucial factors in obtaining efficient SLN and NLC formulations [27–30].

On the other hand, the therapeutic potential of hemp extracts, including phytocannabinoids, has been the interest of multiple scientists worldwide. *Cannabis sativa* L. is widely recognized as a non-psychoactive constituent with many medical properties for different human diseases. Cannabis-derived cannabidiol (CBD, C<sub>21</sub>H<sub>30</sub>O<sub>2</sub>) belongs to the group of terpenophenols. CBD has potent therapeutic properties (antioxidant, anti-inflammatory, neuroprotective) due to its already confirmed efficiency against neurological diseases or various cancer types, including neoplasms of the neural system [31,32].

The study aimed to load the selected cannabis extract (Figure 1) in both lipid carriers, namely SLN and NLC, assess its effect on the particle size, and determine the encapsulation parameters. The viscoelastic behavior and crystallinity index of the developed particles were also characterized.



Figure 1. Hemp extract (*Cannabis sativa* L.) [own photography].

## 2. Results and Discussion

### 2.1. Chromatography Analysis

The analysis of the hemp extract was performed by the High-Performance Liquid Chromatographic (HPLC), which is a validated technique that enabled quantification of 11 cannabinoids in the *Cannabis sativa* L. extract using a wavelength of 230 nm within 22 min. All analyzed samples belonging to the same variety of *Cannabis sativa* L. did not show significant differences in the concentration of cannabinoids, as shown in Table 1. Slight discrepancies between the analyzed samples were observed, mainly in the content of CBDA (about 7%) and CBD (0.22%). The remaining cannabinoids (CBDV, CBGA, CBG, CBN,  $\Delta^9$ -THC, CBNA, CBC, THCA, and CBCA) had similar concentrations in both samples.  $\Delta^9$ -THC was determined at 0.25%, which is the limit of the permissible concentration value. According to the current regulations on the cultivation of *Cannabis sativa* L. [31,33], the total THC content cannot be higher than 0.2%. The maximum permitted limit for some cannabis varieties should be 0.6%  $\Delta^9$ -THC [31].

Table 1. Percentage of individual cannabinoids in the cannabis samples (based on Supplementary Materials, Figures S1 and S2).

Lp.	1.	2.	3.	4.	5.	6.	7.	8.	9.	10.	11.
Cannabinoid *	CBDV [%]	CBDA [%]	CBGA [%]	CBG [%]	CBD [%]	CBN [%]	$\Delta^9$ -THC [%]	CBNA [%]	CBC [%]	THCA [%]	CBCA [%]
Sample 1	0.07	7.41	0.09	0.06	3.07	0.08	0.25	0.04	0.22	0.38	0.39
Sample 2	0.06	7.09	0.04	0.06	2.97	0.08	0.25	0.04	0.22	0.37	0.38

\* Abbreviations: CBDV—cannabidivarin; CBDA—cannabidiol or cannabidiol acid; CBGA—cannabigerol or cannabigerol acid; CBG—cannabigerol; CBD—cannabidiol; CBN—cannabinol;  $\Delta^9$ -THC—delta-9-tetrahydrocannabinol; CBNA—cannabinol or cannabinoic acid; CBC—cannabichromene; THCA—tetrahydrocannabinolic acid; CBCA—cannabichromene acid.

The results confirmed that the most abundant ingredient was CBDA, followed by CBD. The remaining compounds were present in minimal amounts, ranging from 0.04 to 0.39%. CBDA is found in raw plant matter and is an acidic precursor to active CBD, which is considered the most promising cannabinoid for its properties and applications in medicine. In addition, it is worth underlining that CBGA is a compound from which all other cannabinoids can be biosynthesized [33], the reason for its low concentration detected in both tested samples (0.04–0.09%).

### 2.2. Determination of Particle Size, Polydispersity Index, and Zeta Potential

Once the lipid nanoparticles (SLN and NLC) loaded with CBD were produced, the mean particle size (Z-Ave) and polydispersity index (PDI) of all developed formulations were determined directly after production and up to 30 days. Results on the day of production (day 0) were obtained for the empty-SLN and empty-NLC (both considered

as standard samples) and reached about  $201.5 \pm 3.80$  nm with PDI  $0.281 \pm 0.01$  [n.u.] and  $173.3 \pm 4.40$  nm with PDI  $0.235 \pm 0.02$  [n.u.], respectively.

CBD-cSLN suspensions, containing 4% (*w/w*) of solid lipid (Compritol® 888 ATO), 1.5% (*w/w*) of surfactant (Poloxamer® 188) and 1% (*w/w*) of active compound (CBD extract), were produced using a probe sonication and stored at room temperature (25 °C) for 30 days. Then, Z-Ave, PDI, and zeta potential (ZP) were measured 1, 14, and 30 days after production. The results are presented in Figure 2. As a result, the Z-Ave for CBD-cSLN suspensions varied from  $217.2 \pm 6.50$  nm (day 1) with a PDI of  $0.273 \pm 0.02$  [n.u.]. Furthermore, after two weeks of storage at 25 °C, the particle size of cSLN suspensions loaded with CBD extract increased to  $227.7 \pm 11.10$  nm (day 14) with a PDI of  $0.301 \pm 0.02$  [n.u.]. It can indicate a slight agglomeration process. Finally, four weeks after the production, the CBD-cSLN suspensions gained  $222 \pm 5.00$  nm (day 30) with a PDI of  $0.320 \pm 0.01$  [n.u.].

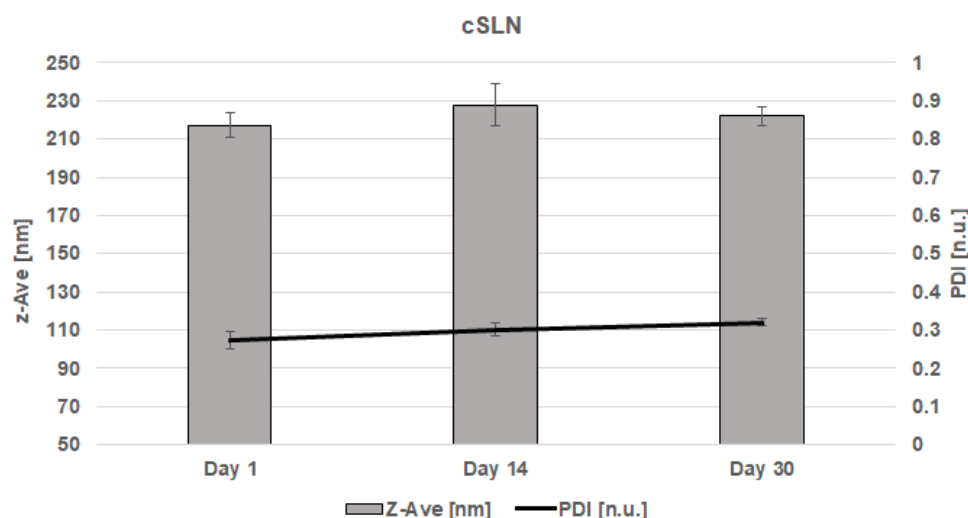


**Figure 2.** Z-Ave and PDI for CBD-cSLN on the 1, 14, and 30 days after the production.

Zeta potential (ZP) of empty cSLN was  $-18.09 \pm 0.81$  [mV], whereas of CBD-cSLN was  $-12.99 \pm 0.90$  [mV] (day 0) to  $-12.42 \pm 2.14$  [mV] (day 30). All of the results are presented in Table 2. It may indicate that the non-ionic nature of the surfactant has formed a spherically stabilizing adsorbed polymer layer in the SLN surface [34].

**Table 2.** ZP for CBD-cSLN and CBD-cNLC on the 1 and 30 days after the production.

Sample Name	Measurement Time (Days after Production)	ZP [mV] ± SD
empty-cSLN	0	$-18.09 \pm 0.81$
CBD-cSLN	1	$-12.99 \pm 0.90$
	30	$-12.42 \pm 2.14$
empty-cNLC	0	$-13.63 \pm 0.89$
CBD-cNLC	1	$-5.51 \pm 1.58$
	30	$-12.06 \pm 1.50$

Abbreviations: SD—Standard Deviation.

CBD-cNLC suspensions, consisting of 3% (*w/w*) of solid lipid (Compritol® 888 ATO), 1% (*w/w*) of liquid lipid (Miglyol® 812), 1.5% (*w/w*) of surfactant (Poloxamer® 188) and 1% (*w/w*) of active compound (CBD extract), were also produced using a probe sonication and stored at room temperature for 30 days. The Z-Ave and PDI were measured 1, 14, and 30 days after production. Figure 3 shows that the Z-Ave for CBD-cSLN suspensions varied from  $158.3 \pm 6.60$  nm (day 1), with a PDI of  $0.325 \pm 0.02$  [n.u.]. Two weeks later, the particle size of cSLN suspensions loaded with CBD extract stored at 25 °C decreased to  $128.6 \pm 3.10$  nm (day 14) with a PDI of  $0.327 \pm 0.01$  [n.u.]. After one month after the

production, the CBD-cSLN suspensions amounted to  $146.2 \pm 2.10$  nm (day 30) with a PDI of  $0.340 \pm 0.01$  [n.u.].

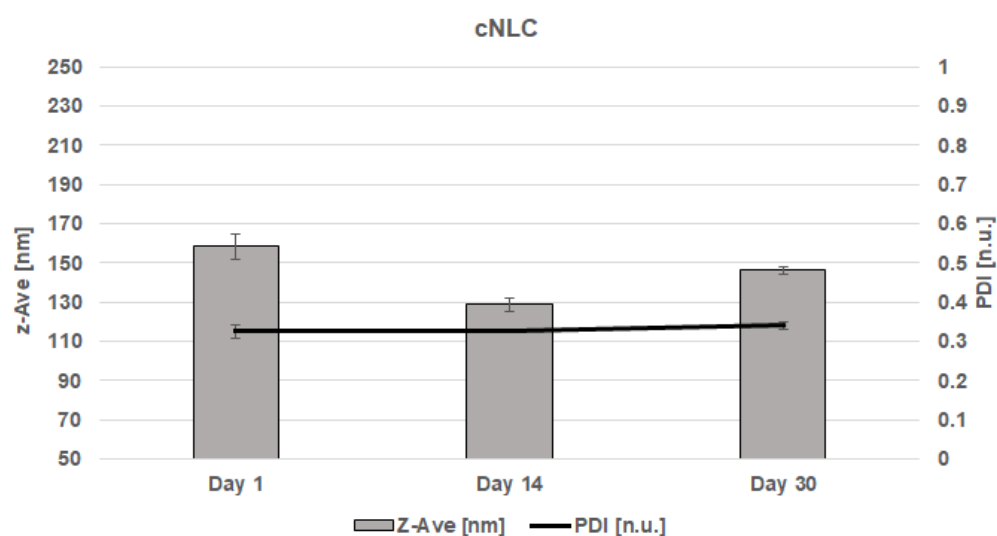


**Figure 3.** Z-Ave and PDI for CBD-cNLC on the 1, 14, and 30 days after the production.

Zeta potential (ZP) of empty cNLC was recorded at  $-13.63 \pm 0.89$  [mV], whereas of CBD-cNLC was recorded at  $-5.51 \pm 1.58$  mV (day 0) to  $-12.06 \pm 1.50$  mV (day 30). Results are also presented in Table 3. Similar to empty-cSLN and CBD-cSLN, empty-cNLC and CBD-cNLC also showed that the presence of active compounds decreased the stability of the samples.

**Table 3.** Encapsulation efficiency (EE%) and loading capacity (LC%) for CBD-cSLN, CBD-cNLC.

	CBD-cSLN	CBD-cNLC
EE [%]	74.23	70.44
LC [%]	15.77	15.11

Zeta potential is a physical property exhibited by any particle in suspension, macromolecule, or material surface. A significant positive or negative value of the zeta potential of nanoparticles indicates good physical stability due to electrostatic repulsion. The dissociation of acidic groups on the surface of a particle will give rise to a negatively charged surface. Conversely, a primary surface will take on a positive charge. In both cases, the magnitude of the surface charge depends on the acidic or basic strengths of the surface groups and the pH of the solution. The surface charge can be reduced to zero by suppressing the surface ionization by decreasing the pH of negatively charged particles or increasing the pH of positively charged particles. The general dividing line between stable and unstable suspensions is generally taken at either +30 or −30 mV. Particles with zeta potentials more positive than +30 mV or more negative than −30 mV usually are considered stable. In our present case, our particles were slightly negative, showing that it is not the surface electrical charge that contributes to the physical stability of the particles, but rather the stereochemical hindrance promoted by the surfactants surrounding the particles.

The final size may depend on various factors, such as the chemical structure of the lipids and surfactants composing the systems and their chemical interaction. It should be pointed out that the largest particle size on day 14 corresponded to CBD-cSLN containing Compritol® 888 ATO as solid lipid. NLC suspensions either consisted of one solid lipid or liquid lipid and showed significantly smaller particle size than cSLN. This could be attributed to the structural differences between lipid nanoparticles and the inclusion of Miglyol® 812 in the cNLC formulations. In addition to that, PDI was similar in all CBD-loaded nanoparticles and varied in the optimal range from 0.2 to 0.3 [n.u.]. The

stereochemical stability of lipid nanoparticles was monitored for 30 days. Additionally, previous research has revealed that the concentration of Miglyol<sup>®</sup> 812 remarkably impacts the nanoemulsions' stability, which is a crucial factor influencing particle size [35]. The slight reduction in particle size with the loading of CBD was attributed to the bonds between the CBD molecule and solid and liquid lipids, resulting in an imperfect crystal-type of NLC. It involves mixing spatially different lipids, consisting of many fatty acids, which introduce imperfections in the order of the crystals. The drug loading can further increase the molecular interactions, resulting in a smaller nanoparticle size.

### 2.3. Encapsulation Efficiency and Loading Capacity

The encapsulation efficiency (EE%) and loading capacity (LC%) were determined as qualitative and quantitative parameters of the production of process. EE and LC were calculated for CBD-cSLN and CBD-cNLC formulations to estimate how much CBD was inside each system. The results are shown in Table 3. The influence of varying lipid types (Compritol<sup>®</sup> 888 ATO and Miglyol<sup>®</sup> 812) on the more efficient loading CBD was analyzed. Consequently, CBD-cSLN achieved the EE of 74.23%, CBD-cNLC gained 70.44%, and the LC was 15.77% and 15.11%, respectively.

### 2.4. Rheology Study

The viscosity of the lipid nanoparticle-based formulations can vary from liquids to semi-solid systems. It also governs the selection of the ideal pharmaceutical formulation for the intended administration route. When nanodispersions are applied to the skin, they should show a thixotropic pattern with a high viscosity. Therefore, they can adhere and be retained on the skin site. On the other hand, in oral formulations, lipid nanoparticle-based dispersions can be used as granulating media in tablet production to convert the powder into a viscoelastic mass and then into dry-looking granules or load soft and hard gelatin capsules (either as liquids or after spray/freeze-dried).

To study the rheological behavior of the dispersions, an oscillation frequency sweep test was run for each formulation (CBD-cSLN, CBD-cNLC) at  $22 \pm 0.5$  °C one day after production, over the frequency range of 0–10 Hz. For comparison purposes between CBD-cSLN (Figure 4, left) and CBD-cNLC (Figure 4, right), we recorded the storage modulus ( $G'$ ), loss modulus ( $G''$ ), and shear viscosity. The loss modulus was higher than the storage modulus over the applied frequency range for both lipid nanoparticle-based formulations. The storage modulus (viscous component) resembles how much energy the dispersion requires to be distorted, whereas the loss modulus (elastic component) translates the energy lost during the strain. At low frequencies, the shear rate is also low, which means that the capacity of the dispersions to maintain their original media strength is high. With the increase in the frequency range, the shear rate also increases, thus requiring more energy and consequently increasing the viscous component ( $G'$ , storage modulus).

The results showed that  $G''$  was always higher than  $G'$  for both tested samples. It means that they were more elastic than viscous. When the stress was removed, the dispersions were restored to equilibrium but did not follow the same conformational path. Moreover, the dispersions did not maintain their shape, and this behavior is typical of a liquid-like character system.

In turn, the rise in the frequency increased the shear viscosity for CBD-cSLN (Figure 4, left), while for CBD-cNLC, the reverse was observed (Figure 4, right). The addition of an oily component (Miglyol<sup>®</sup> 812) to the solid matrix of SLN (to obtain NLC) could result in more viscous dispersions, as seen with the higher shear viscosity values recorded for CBD-cNLC when compared to CBD-cSLN.

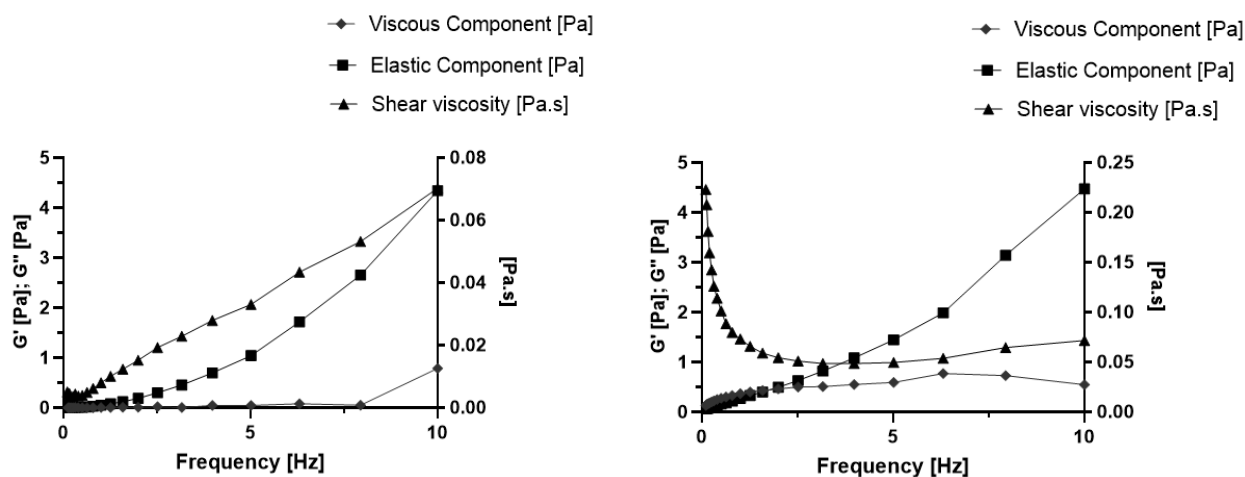


**Figure 4.** Rheological behavior of CBD-cSLN (left-hand) and CBD-cNLC (right-hand) over a frequency range of 0–10 Hz.

### 2.5. DSC

The thermodynamic stability of cSLN and cNLC is mainly governed by the lipid modifications encountered upon loading with the active ingredient. The selected solid lipid was Compritol (i.e., glyceryl behenate), a mixture of mono-, di- and tri-behenate of glycerol [36]. It is reported that Compritol has a typical crystalline structure of triglycerols, containing tiny amounts of  $\alpha$ -form [37]. The crystallinity index, which measures the amount of solid content inside the particles, shows the slightly solid character of SLN compared to NLC, as documented in the literature [38].

The production of SLN and NLC loading CBD resulted in the decrease in the melting peak down to 71.0 °C and 63.6 °C, respectively, with a significant depression of the crystallization index when we compare CBD-cSLN (90.41%) with CBD-cNLC (40.18%) (Table 4). These results are aligned with the loading capacity and encapsulation efficiency encountered for these particles.

**Table 4.** DSC parameters for CBD-cSLN and CBD-cNLC.

DSC Parameters	CBD-cSLN	CBD-cNLC
Peak Maximum (°C)	71.00	63.60
Enthalpy (J/g)	3.960	1.934
Crystallinity Index (%)	90.41	40.18

Figure 5 shows bulk Compritol melted at 75.8 °C, with a recording melting enthalpy of 109.7 J/g. The bulk CBD analysis showed the active ingredient's low melting peak at 37.5 °C (Figure 6). It has been loaded into lipid nanoparticles, contributing to the crystallinity index recorded for both types of particles.

### 2.6. SEM

The loading of CBD into Compritol-composed SLN and NLC did not compromise the typical round and smooth surface of nanoparticles, as confirmed by SEM analyses. Figures 7 and 8 depict the images recorded for both developed formulations at different resolutions. These results corroborate the solid character of both types of particles described in Table 5 and the small mean particle size and polydispersity index shown in Tables 2 and 3. These features are responsible for the typical rheological behavior of monodispersed nanoparticle dispersions.

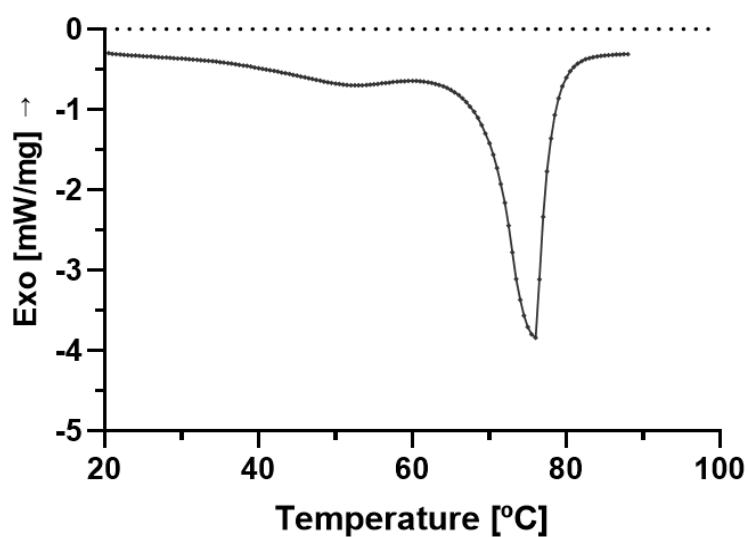


**Figure 5.** Differential scanning calorimetric profile of bulk Compritol, depicting a melting peak at 75.8 °C, with an onset temperature of 61.8 °C and end set at 84.4 °C.

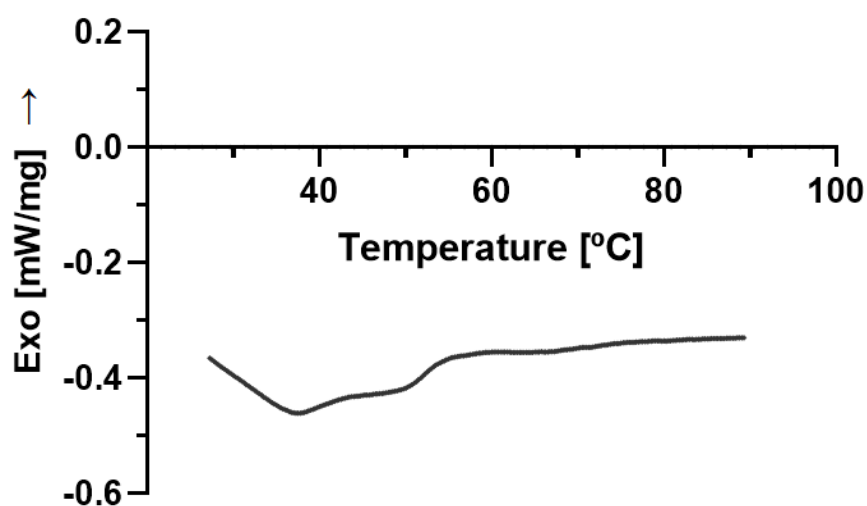


**Figure 6.** Differential scanning calorimetric profile of bulk CBD, depicting a melting peak at 37.5 °C.

**Table 5.** The lipid nanoparticle dispersions (% *w/w*) were composed of Compritol<sup>®</sup> 888 ATO (solid lipid) to obtain CBD-cSLN and CBD-cNLC.

Ingredients	Formulation	
	CBD-cSLN	CBD-cNLC
CBD	1	1
Compritol <sup>®</sup> 888 ATO	4	3
Miglyol <sup>®</sup> 812	-	1
Poloxamer <sup>®</sup> 188	1.5	1.5
Water	93.5	93.5

Abbreviations: CBD—cannabidiol; cSLN—solid lipid nanoparticles-based Compritol 888 ATO; cNLC—nanostructured lipid carriers-based Compritol 888 ATO; Miglyol<sup>®</sup> 812—medium-chain triglycerides extracted from endosperms of palm oil and coconut plants; Poloxamer<sup>®</sup> 188—2-(2-propoxypropoxy) ethanol, nonionic block linear copolymer.



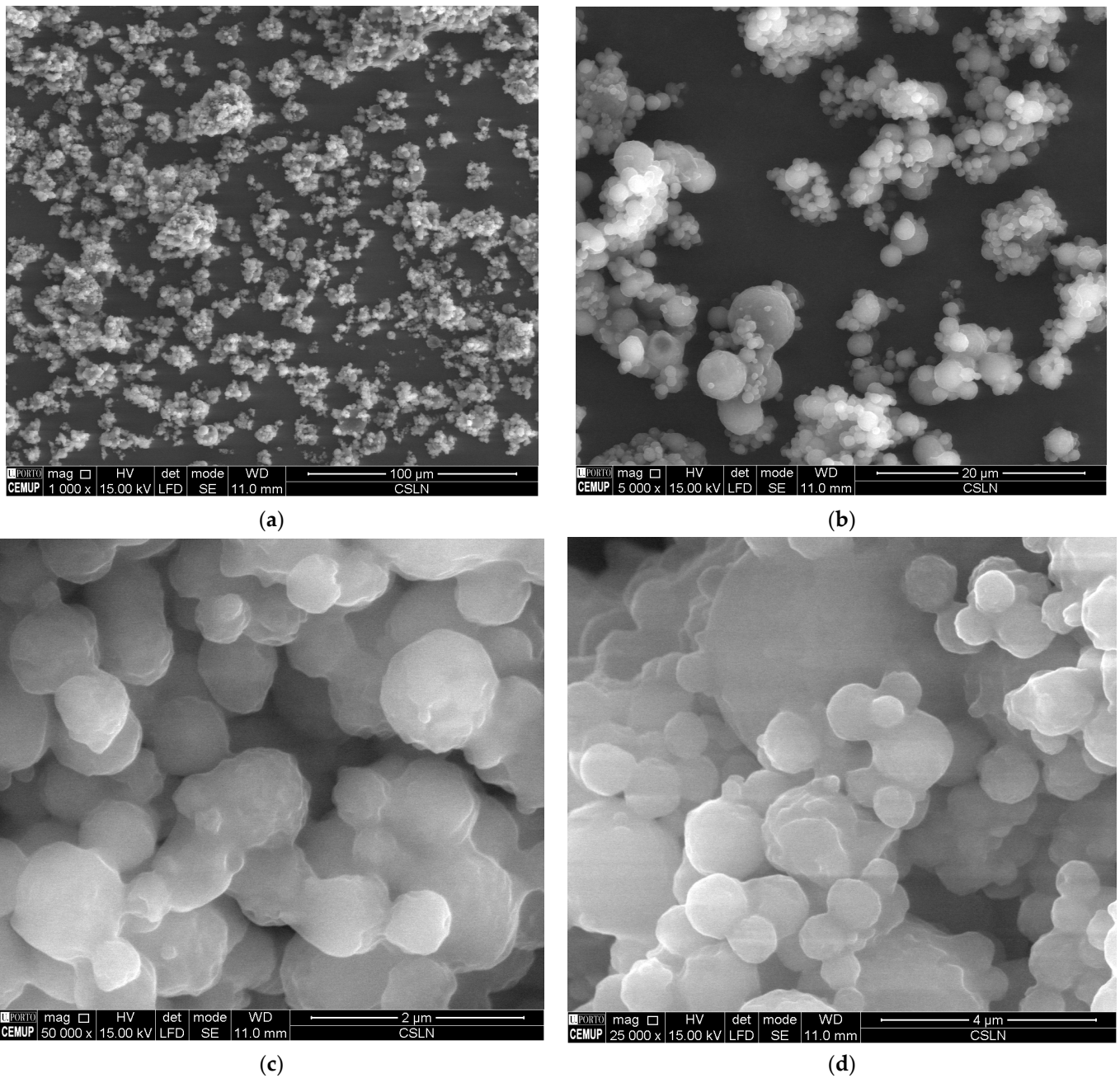


**Figure 7.** Scanning electron microscopy analysis of CBD-loaded cSLN at different resolutions, (a) 1000 $\times$ , (b) 5000 $\times$ , (c) 25,000 $\times$ , and (d) 50,000 $\times$ .

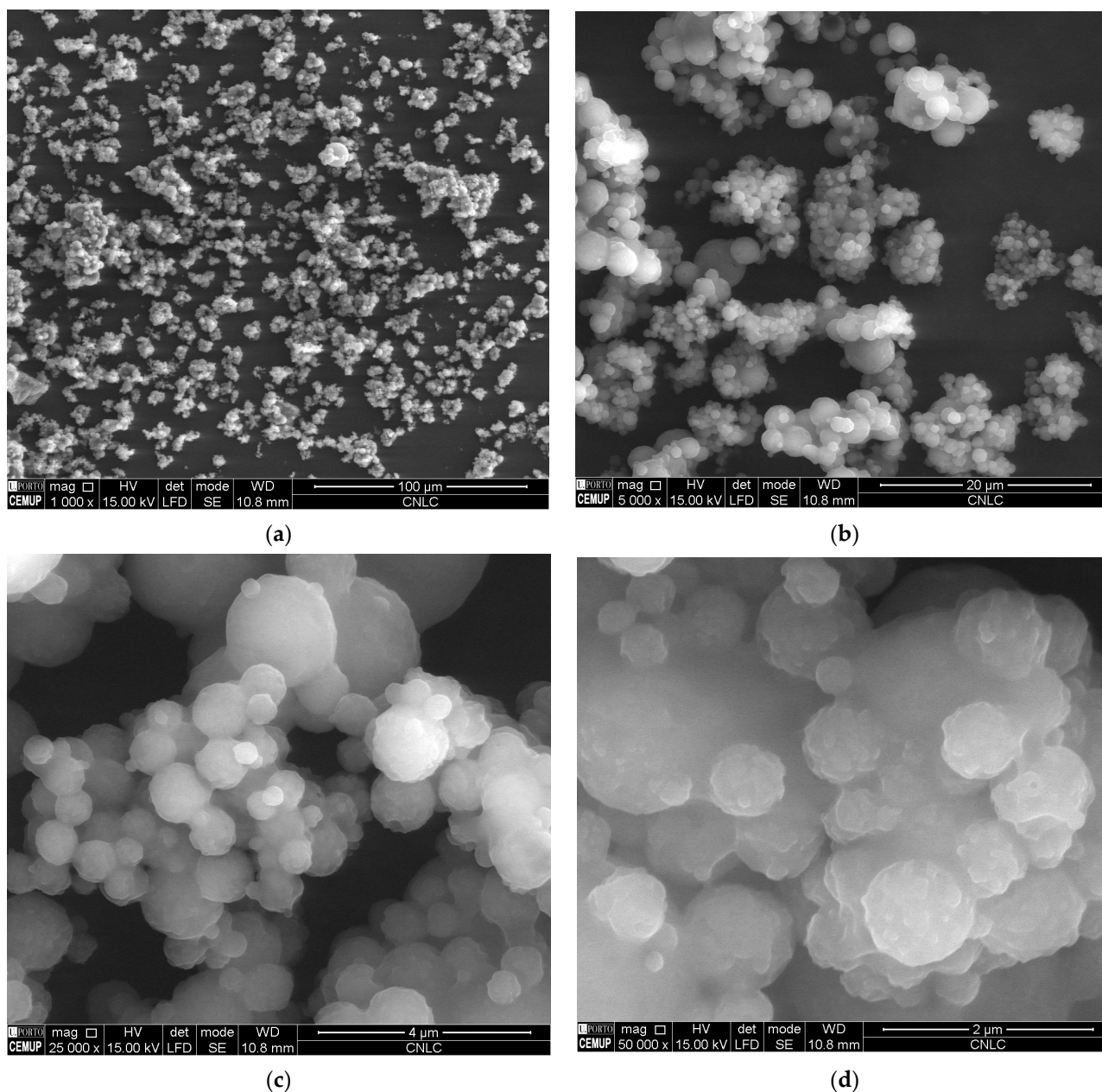


**Figure 8.** Scanning electron microscopy analysis of CBD-loaded cNLC at different resolutions, (a) 1000 $\times$ , (b) 5000 $\times$ , (c) 25,000 $\times$ , and (d) 50,000 $\times$ .

### 3. Materials and Methods

#### 3.1. Plant Extract Preparation

A hemp extract was prepared using panicles of Hungarian monoecious hemp variety KC Dora (extract B) and Polish monoecious hemp variety Tygra. Hemp was cultivated in experimental plots (Institute of Natural Fibres & Medicinal Plants). Cultivation conditions included nitrogen fertilization (30 kg/ha) and seed sowing density (30 kg of seeds/ha). Panicles were harvested at the late flowering stage when the highest content of cannabinoid compounds in dried plant material was observed (CBD—1.9153% and THC—0.0681%). The hemp extract was prepared in two-phase solvent extraction. The plant material was exposed to an organic solvent at 30 °C, and the resulting extract was concentrated in an evaporator (50 mbar vacuum). Subsequently, the extract was dissolved in ethanol and water at 80 °C. After ethanol evaporation, the extract was concentrated again (50 mbar,

vacuum). The final stage of the process was decarboxylation (temperature 130 °C), which resulted in the extract containing 215.2 mg/g CBD and 13.3 mg/g THC.

### 3.2. Chromatography of Plant Extract

Approximately 150 mg of the sample was weighed into a centrifuge tube and flooded with precisely 10 mL of a MeOH: THF mixture. Then, it was shaken for 30 min, and the tubes were centrifuged at 5500 rpm. Samples were diluted 10-fold into an HPLC-type vial and placed on an HPLC autosampler. All analyzes were performed on a gradient of 0.1% H<sub>3</sub>PO<sub>4</sub> in water with CAN, observing UV light absorbance at 230 nm on a chromatographic column with a stationary phase C18. Identification and calculation of concentration for cannabinoids were performed based on the chromatograms of the standards, from which the calibration curves were plotted.

### 3.3. Production of SLN and NLC

SLN and NLC were produced by hot high-pressure homogenization as described by Doktorovova et al. [39] with slight modification and based on preliminary studies as described by Souto et al. [40]. Briefly, the melted lipid phase (solid lipid in case of SLN; solid lipid and liquid lipid in case of NLC) was dispersed in the aqueous surfactant solution heated at the same temperature using a probe sonication (Sonics Vibracell, Newtown, CT, USA) for 15 min and 70% amplitude. A hot emulsion was obtained, then left to cool down at room temperature. For the loading of CBD, the extract was added to the inner oil phase before emulsification. The composition of the developed batches is shown in Table 5.

### 3.4. Formulation Characterization

#### 3.4.1. Particle Size, Polydispersity, and Zeta Potential

In this work, dynamic light scattering (DLS) analysis (NanoBrook Omni, Brookhaven Instruments, Holtsville, NY, USA) was used to record the mean particle size (Z-Ave, polydispersity index (PDI), and zeta potential (ZP). The samples were diluted in MilliQ water 1:10 v/v and analyzed at 20 °C, with a refractive index of 1.331 and a dielectric constant of 80.37. All of Z-Ave, PDI, and ZP measurements were recorded in triplicate.

#### 3.4.2. Encapsulation Efficiency and Loading Capacity

A volume of 5 mL of the obtained particles was submitted at centrifugation by Amicon® Ultra Centrifugal Filters Ultracel (Millipore, Germany) for 25 min at 4500 rpm to isolate the particles from the suspension. This analysis aimed to estimate the CBD encapsulation efficiency. The supernatant was quantified against a calibration curve ( $y = 3.5316x + 0.0043$ ,  $R^2 = 0.9980$ ) to determine the drug concentration. The calibration curve standards were prepared by diluting the CBD in acetone to ensure total dilution. The concentration of each standard of the calibration curve and the filtrate concentration were measured in a BioTek Synergy HT plate reader (BioTek Instruments, Winooski, VT, USA) at 327 nm. The encapsulation efficiency (EE) and loading capacity (LC) of CBD loaded SLN/NLC were calculated as follows [41]:

$$EE\% = \frac{W_{CBD} - W_S}{W_{CBD}} \times 100$$

$$LC\% = \frac{W_{CBD} - W_S}{W_{CBD} - W_S + W_L} \times 100$$

where  $W_{CBD}$  is the mass of CBD used to produce the loaded nanoemulsions,  $W_S$  is the mass of CBD quantified in the supernatant, and  $W_L$  is the weight of lipid added in the formulation. Centrifugal filter units ( $\mu$ L) were used with a cut-off of 50 kDa, i.e., 50,000 nominal molecular weight limits (NMWL).

### 3.4.3. Rheology

The rheology studies were conducted on a Malvern Kinexus rheometer (Malvern Instruments, UK). The oscillation frequency sweep test was applied over a frequency range from 0 to 10 Hz. The storage modulus ( $G'$ ), loss modulus ( $G''$ ), and the complex viscosity ( $\eta^*$ ) of lipid nanoparticles were described as a function of the frequency at a constant stress amplitude of 5 Pa (linear viscoelastic region). All measurements were carried out directly at room temperature (25 °C).

### 3.4.4. Differential Scanning Calorimetry (DSC)

This study used a differential scanning calorimeter, DSC 200 F3 Maia Differential Scanning Calorimeter from NETZSCH Premier Technologies. The liquid nitrogen's temperature range extends from  $-150$  °C to  $600$  °C. The heat flux sensor of this equipment allows high stability, improved resolution, and fast response time. Laser-guided welding processes for the sensor disk and thermocouple wires yield high sensitivity and robustness. In this work, the difference between the temperature of the samples and the standard was recorded. The samples of CBD-loaded SLN/NLC were scanned from  $25$  to  $90$  °C/min. The crystallization index (CI, %) was determined using the following equation [38]:

$$CI(\%) = \frac{\Delta H_{\text{SLN or NLC aqueous dispersion}}}{\Delta H_{\text{bulk material}} \times \text{Concentration}_{\text{lipid phase}}} \times 100$$

where  $\Delta H$  is the molar melting enthalpy given by J/g, the percentage of the lipid phase gives the concentration.

### 3.4.5. Scanning Electron Microscopy

The scanning electron microscopy (SEM) analysis was performed in a high-resolution Scanning Electron Microscope (JEOL JSM-6390 Scanning Electron Microscope (SEM) at an accelerating voltage of 20 kV, Tokyo, Japan). The CBD-loaded SLN and NLC were coated with platinum (20 nm thick) using an Ion Sputter (JFC-1100, JEOL Ltd.) (Tokyo, Japan) for 5 min at 20 mA. The magnification was set at 10,000.

## 4. Conclusions

In the present work, cannabis extract was successfully loaded into two types of lipid nanoparticles, namely SLN and NLC. While the loading capacity of the extract in both systems remained around 15%, the EE was slightly higher for SLN (ca. 75%) than for NLC (ca. 70%). On the other hand, both SLN and NLC showed interesting crystallinity indices, anticipating the reason for the relatively high encapsulation efficiencies. The lipid nanoparticle dispersions followed a typical viscoelastic behavior of liquids, so further technological processing will be needed to develop a final pharmaceutical product.

**Supplementary Materials:** The following supporting information can be downloaded at: <https://www.mdpi.com/article/10.3390/molecules28062875/s1>, Figure S1: Sample 1 and chromatographic analysis of a cannabinoid extract containing a mixture of cannabinoids. Figure S2: Sample 2 and chromatographic analysis of a cannabinoid extract containing a mixture of cannabinoids.

**Author Contributions:** A.Z., R.d.A., J.F., F.F. and E.B.S. contributed to the conceptualization, methodology, validation, formal analysis, investigation, and writing—original draft preparation. A.Z., F.F., M.B.P.P.O., M.S., K.W., R.S. and J.K. contributed to data validation, literature review, and software management. A.Z., M.B.P.P.O., R.S., J.K. and E.B.S. contributed to the writing—review and editing, project administration, resources, supervision, and funding acquisition. All authors have made a substantial contribution to the work. All authors have read and agreed to the published version of the manuscript.

**Funding:** This research was funded by the Institute of Human Genetics, Polish Academy of Sciences by an internal grant for the implementation of a single scientific activity by the National Science Centre within the MINIATURA 4 for single research activity (2020/04/X/ST5/00789), and by the START 2021 Program of the Foundation for Polish Science (FNP) both granted to Aleksandra Zielińska. This research was also supported by the National Centre for Research and Development (grant number INNOMED/I/11/NCBR/2014) from the Innovative Economy Operational Programme funds within the framework of the European Regional Development Fund. The research was also supported by the Fundação para a Ciência e a Tecnologia (FCT) through the scholarship 2020.04729.BD granted to Raquel da Ana.

**Institutional Review Board Statement:** Not applicable.

**Informed Consent Statement:** Not applicable.

**Data Availability Statement:** Not applicable.

**Acknowledgments:** The authors are most grateful to René Beyer, Head of Strategic Sales Pharma of IOI Oleo GmbH Company in Germany, for gifting the solid lipids used in the study. Faezeh Fathi is grateful to Laboratório Associado para a Química Verde—Tecnologias e Processos Limpos—UIDB/50006/2020 that supports her grant REQUIMTE 2020-20. The authors are thankful to Salette Reis from the Chemical Sciences Department University of Porto (FFUP) for providing the equipment. Eliana B. Souto acknowledges the national funds from FCT—Fundação para a Ciência e a Tecnologia, I.P., in the scope of the project UIDP/04378/2020 and UIDB/04378/2020 of the 415 Research Unit on Applied Molecular Biosciences—UCIBIO and the project LA/P/0140/2020 of the 416 Associate Laboratory Institute for Health and Bioeconomy—i4HB.

**Conflicts of Interest:** The authors declare no conflict of interest.

## References

1. Souto, E.B.; Baldim, I.; Oliveira, W.P.; Rao, R.; Yadav, N.; Gama, F.M.; Mahant, S. SLN and NLC for topical, dermal, and transdermal drug delivery. *Expert Opin. Drug Deliv.* **2020**, *17*, 357–377. [[CrossRef](#)] [[PubMed](#)]
2. Mahant, S.; Rao, R.; Souto, E.B.; Nanda, S. Analytical tools and evaluation strategies for nanostructured lipid carrier-based topical delivery systems. *Expert Opin. Drug Deliv.* **2020**, *17*, 963–992. [[CrossRef](#)] [[PubMed](#)]
3. Doktorovova, S.; Kovacevic, A.B.; Garcia, M.L.; Souto, E.B. Preclinical safety of solid lipid nanoparticles and nanostructured lipid carriers: Current evidence from in vitro and in vivo evaluation. *Eur. J. Pharm. Biopharm.* **2016**, *108*, 235–252. [[CrossRef](#)] [[PubMed](#)]
4. Doktorovova, S.; Souto, E.B.; Silva, A.M. Nanotoxicology applied to solid lipid nanoparticles and nanostructured lipid carriers—A systematic review of in vitro data. *Eur. J. Pharm. Biopharm.* **2014**, *87*, 1–18. [[CrossRef](#)]
5. Müller, R.; Petersen, R.; Hommoss, A.; Pardeike, J. Nanostructured lipid carriers (NLC) in cosmetic dermal products. *Adv. Drug Deliv. Rev.* **2007**, *59*, 522–530. [[CrossRef](#)]
6. Lippacher, A.; Müller, R.; Mäder, K. Liquid and semisolid SLN<sup>TM</sup> dispersions for topical application: Rheological characterization. *Eur. J. Pharm. Biopharm.* **2004**, *58*, 561–567. [[CrossRef](#)]
7. Rashidi, L. Different nano-delivery systems for delivery of nutraceuticals. *Food Biosci.* **2021**, *43*, 101258. [[CrossRef](#)]
8. Mohammadi, M.; Assadpour, E.; Jafari, S.M. Encapsulation of food ingredients by nanostructured lipid carriers (NLCs). In *Lipid-based Nanostructures for Food Encapsulation Purposes*; Elsevier: Amsterdam, The Netherlands, 2019; pp. 217–270.
9. Haider, M.; Abdin, S.M.; Kamal, L.; Orive, G. Nanostructured lipid carriers for delivery of chemotherapeutics: A review. *Pharmaceutics* **2020**, *12*, 288. [[CrossRef](#)]
10. Salvi, V.R.; Pawar, P. Nanostructured lipid carriers (NLC) system: A novel drug targeting carrier. *J. Drug Deliv. Sci. Technol.* **2019**, *51*, 255–267. [[CrossRef](#)]
11. Oliveira, D.R.B.; Michelon, M.; de Figueiredo Furtado, G.; Sinigaglia-Coimbra, R.; Cunha, R.L.  $\beta$ -Carotene-loaded nanostructured lipid carriers produced by solvent displacement method. *Food Res. Int.* **2016**, *90*, 139–146. [[CrossRef](#)]
12. Bagherpour, S.; Alizadeh, A.; Ghanbarzadeh, S.; Mohammadi, M.; Hamishehkar, H. Preparation and characterization of Betasitosterol-loaded nanostructured lipid carriers for butter enrichment. *Food Biosci.* **2017**, *20*, 51–55. [[CrossRef](#)]
13. Zheng, M.; Falkeborg, M.; Zheng, Y.; Yang, T.; Xu, X. Formulation and characterization of nanostructured lipid carriers containing a mixed lipids core. *Colloids Surf. A Physicochem. Eng. Asp.* **2013**, *430*, 76–84. [[CrossRef](#)]
14. Cui, S.; Zhang, S.; Ge, S.; Xiong, L.; Sun, Q. Green preparation and characterization of size-controlled nanocrystalline cellulose via ultrasonic-assisted enzymatic hydrolysis. *Ind. Crops Prod.* **2016**, *83*, 346–352. [[CrossRef](#)]
15. Artiga-Artigas, M.; Odriozola-Serrano, I.; Oms-Oliu, G.; Martín-Belloso, O. Nanostructured systems to increase bioavailability of food ingredients. In *Nanomaterials for Food Applications*; Elsevier: Amsterdam, The Netherlands, 2019; pp. 13–33.
16. Lacatusu, I.; Mitrea, E.; Badea, N.; Stan, R.; Oprea, O.; Meghea, A. Lipid nanoparticles based on omega-3 fatty acids as effective carriers for lutein delivery. Preparation and in vitro characterization studies. *J. Funct. Foods* **2013**, *5*, 1260–1269. [[CrossRef](#)]

17. Ali, A.; Ahmad, U.; Akhtar, J.; Khan, M.M. Engineered nano scale formulation strategies to augment efficiency of nutraceuticals. *J. Funct. Foods* **2019**, *62*, 103554. [[CrossRef](#)]
18. Maretti, E.; Pavan, B.; Rustichelli, C.; Montanari, M.; Dalpiaz, A.; Iannuccelli, V.; Leo, E. Chitosan/heparin polyelectrolyte complexes as ion-pairing approach to encapsulate heparin in orally administrable SLN: In vitro evaluation. *Colloids Surf. A Physicochem. Eng. Asp.* **2021**, *608*, 125606. [[CrossRef](#)]
19. Babazadeh, A.; Ghanbarzadeh, B.; Hamishehkar, H. Formulation of food grade nanostructured lipid carrier (NLC) for potential applications in medicinal-functional foods. *J. Drug Deliv. Sci. Technol.* **2017**, *39*, 50–58. [[CrossRef](#)]
20. Gasa-Falcon, A.; Odriozola-Serrano, I.; Oms-Oliu, G.; Martín-Belloso, O. Nanostructured lipid-based delivery systems as a strategy to increase functionality of bioactive compounds. *Foods* **2020**, *9*, 325. [[CrossRef](#)]
21. Luan, J.; Zhang, D.; Hao, L.; Li, C.; Qi, L.; Guo, H.; Liu, X.; Zhang, Q. Design and characterization of Amoitone B-loaded nanostructured lipid carriers for controlled drug release. *Drug Deliv.* **2013**, *20*, 324–330. [[CrossRef](#)]
22. Bashiri, S.; Ghanbarzadeh, B.; Ayaseh, A.; Dehghannya, J.; Ehsani, A. Preparation and characterization of chitosan-coated nanostructured lipid carriers (CH-NLC) containing cinnamon essential oil for enriching milk and anti-oxidant activity. *Lwt* **2020**, *119*, 108836. [[CrossRef](#)]
23. Kovacevic, A.; Savic, S.; Vuleta, G.; Mueller, R.H.; Keck, C.M. Polyhydroxy surfactants for the formulation of lipid nanoparticles (SLN and NLC): Effects on size, physical stability and particle matrix structure. *Int. J. Pharm.* **2011**, *406*, 163–172. [[CrossRef](#)] [[PubMed](#)]
24. Kiss, E.; Bertóti, I.; Vargha-Butler, E. XPS and wettability characterization of modified poly (lactic acid) and poly (lactic/glycolic acid) films. *J. Colloid Interface Sci.* **2002**, *245*, 91–98. [[CrossRef](#)] [[PubMed](#)]
25. Amasya, G.; Ergin, A.D.; Cakirci, O.E.; Ozçelikay, A.T.; Bayindir, Z.S.; Yuksel, N. A study to enhance the oral bioavailability of s-adenosyl-l-methionine (SAME): SLN and SLN nanocomposite particles. *Chem. Phys. Lipids* **2021**, *237*, 105086. [[CrossRef](#)] [[PubMed](#)]
26. Aburahma, M.H.; Badr-Eldin, S.M. Compritol 888 ATO: A multifunctional lipid excipient in drug delivery systems and nanopharmaceuticals. *Expert Opin. Drug Deliv.* **2014**, *11*, 1865–1883. [[CrossRef](#)]
27. Real, D.A.; Hoffmann, S.; Leonardi, D.; Goycoolea, F.M.; Salomon, C.J. A quality by design approach for optimization of Lecithin/Span®80 based nanoemulsions loaded with hydrophobic drugs. *J. Mol. Liq.* **2021**, *321*, 114743. [[CrossRef](#)]
28. Chun, J.Y.; Kang, H.K.; Jeong, L.; Kang, Y.O.; Oh, J.-E.; Yeo, I.-S.; Jung, S.Y.; Park, W.H.; Min, B.-M. Epidermal cellular response to poly (vinyl alcohol) nanofibers containing silver nanoparticles. *Colloids Surf. B Biointerfaces* **2010**, *78*, 334–342. [[CrossRef](#)]
29. Fanguero, J.F.; Andreani, T.; Egea, M.A.; Garcia, M.L.; Souto, S.B.; Souto, E.B. Experimental factorial design applied to mucoadhesive lipid nanoparticles via multiple emulsion process. *Colloids Surf. B Biointerfaces* **2012**, *100*, 84–89. [[CrossRef](#)]
30. Gonzalez-Mira, E.; Egea, M.; Souto, E.; Calpena, A.; García, M. Optimizing flurbiprofen-loaded NLC by central composite factorial design for ocular delivery. *Nanotechnology* **2010**, *22*, 045101. [[CrossRef](#)]
31. Andrzejewska, A.; Staszak, K.; Kaczmarek-Ryś, M.; Słomski, R.; Hryhorowicz, S. Understanding cannabinoid receptors: Structure and function. *Acta Univ. Lodz. Folia Biol. Oecologica* **2018**, *14*, 1–13. [[CrossRef](#)]
32. Hryhorowicz, S.; Kaczmarek-Ryś, M.; Zielińska, A.; Scott, R.J.; Słomski, R.; Pławski, A. Endocannabinoid System as a Promising Therapeutic Target in Inflammatory Bowel Disease—A Systematic Review. *Front. Immunol.* **2021**, *12*, 790803. [[CrossRef](#)]
33. Brighenti, V.; Pellati, F.; Steinbach, M.; Maran, D.; Benvenuti, S. Development of a new extraction technique and HPLC method for the analysis of non-psychoactive cannabinoids in fibre-type Cannabis sativa L.(hemp). *J. Pharm. Biomed. Anal.* **2017**, *143*, 228–236. [[CrossRef](#)]
34. Shah, M.; Agrawal, Y. Ciprofloxacin hydrochloride-loaded glyceryl monostearate nanoparticle: Factorial design of Lutrol F68 and Phospholipon 90G. *J. Microencapsul.* **2012**, *29*, 331–343. [[CrossRef](#)]
35. Le Bars, G.; Dion, S.; Gauthier, B.; Mhedhbi, S.; Pohlmeier-Esch, G.; Comby, P.; Vivian, N.; Ruty, B. Oral toxicity of Miglyol 812® in the Göttingen®minipig. *Regul. Toxicol. Pharmacol.* **2015**, *73*, 930–937. [[CrossRef](#)]
36. Brubach, J.B.; Jannin, V.; Mahler, B.; Bourgaux, C.; Lessieur, P.; Roy, P.; Ollivon, M. Structural and thermal characterization of glyceryl behenate by X-ray diffraction coupled to differential calorimetry and infrared spectroscopy. *Int. J. Pharm.* **2007**, *336*, 248–256. [[CrossRef](#)]
37. Chawla, V.; Saraf, S.A. Glyceryl Behenate and Its Suitability for Production of Aceclofenac Solid Lipid Nanoparticles. *J. Am. Oil Chem. Soc.* **2011**, *88*, 119–126. [[CrossRef](#)]
38. Campos, J.R.; Fernandes, A.R.; Sousa, R.; Fanguero, J.F.; Boonme, P.; Garcia, M.L.; Silva, A.M.; Naveros, B.C.; Souto, E.B. Optimization of nimesulide-loaded solid lipid nanoparticles (SLN) by factorial design, release profile and cytotoxicity in human Colon adenocarcinoma cell line. *Pharm. Dev. Technol.* **2019**, *24*, 616–622. [[CrossRef](#)]
39. Doktorovova, S.; Silva, A.M.; Gaivao, I.; Souto, E.B.; Teixeira, J.P.; Martins-Lopes, P. Comet assay reveals no genotoxicity risk of cationic solid lipid nanoparticles. *J. Appl. Toxicol.* **2014**, *34*, 395–403. [[CrossRef](#)]

40. Souto, E.B.; Doktorovova, S.; Zielinska, A.; Silva, A.M. Key production parameters for the development of solid lipid nanoparticles by high shear homogenization. *Pharm. Dev. Technol.* **2019**, *24*, 1181–1185. [[CrossRef](#)]
41. Souto, E.B.; Zielinska, A.; Souto, S.B.; Durazzo, A.; Lucarini, M.; Santini, A.; Silva, A.M.; Atanasov, A.G.; Marques, C.; Andrade, L.N.; et al. (+)-Limonene 1,2-Epoxy-Loaded SLNs: Evaluation of Drug Release, Antioxidant Activity, and Cytotoxicity in an HaCaT Cell Line. *Int. J. Mol. Sci.* **2020**, *21*, 1449. [[CrossRef](#)]

**Disclaimer/Publisher's Note:** The statements, opinions and data contained in all publications are solely those of the individual author(s) and contributor(s) and not of MDPI and/or the editor(s). MDPI and/or the editor(s) disclaim responsibility for any injury to people or property resulting from any ideas, methods, instructions or products referred to in the content.